# Publication II

**Arttu Polojärvi and Jukka Tuhkuri. Velocity effects in laboratory scale punch through experiments. *Cold Regions Science and Technology*, 70, 81-93, 2012.**

Cold Regions Science and Technology 70 (2012) 81–93

Contents lists available at SciVerse ScienceDirect

Cold Regions Science and Technology

journal homepage: www.elsevier.com/locate/coldregions

# Velocity effects in laboratory scale punch through experiments

Arttu Polojärvi *, Jukka Tuhkuri

*Aalto University, School of Engineering, Department of Applied Mechanics, P.O.Box 14300, FI-00076 Aalto, Finland*

ARTICLE INFO

*Article history:*
Received 6 May 2011
Accepted 10 September 2011

*Keywords:*
Model scale experiments
Punch through tests
Rubble shear strength measures
Loading rate effects

ABSTRACT

Laboratory scale punch through tests on floating rubble consisting of plastic blocks were conducted. The motivation of using plastic blocks was to simplify the interpretation of results as the plastic blocks do not freeze together. The emphasis was on the methods used to derive the rubble material properties from results. In the experiments, a flat indentor platen penetrated the rubble. The indentor force as a function of its penetration was recorded. Different indentor velocities were used. The behavior of the rubble was related to the measured indentor force records. The results were compared with earlier laboratory scale punch through tests. The experiments showed, that punch through tests give results, that in some cases are difficult to interpret. The reason for this is mainly in the hydrodynamical effects arising with high indentor velocities. The results showed, that the existence of the rubble in the basin could change the hydrodynamical effects from the tests earlier used to capture them. It is shown that these effects can partly explain the shear rate dependency of the ice rubble observed in earlier work on punch through tests.



## 1. Introduction

Punch through tests are used in the development of material models for ice rubble. In a punch through test, a flat indentor moves down and penetrates into the rubble. As one result, the indentor force $F_I$ is achieved during the penetration. From the dimensions of the experimental set-up, and the rubble deformation and failure mechanism during the penetration, some material properties can be derived for the rubble.

For engineering purposes, often the shear strength $\tau$ of the ice rubble is of interest. A common practice in limit load calculations for ice ridge keels has been to use soil mechanics analog and Mohr–Coulomb yield criterion, in which $\tau$ is linearly dependent on the effective compressive stress $\sigma'$ through relation

$$\tau = c + \sigma' \tan\varphi, \tag{1}$$

where $c$ is the cohesion and $\varphi$ is the friction angle. For the derivation of $c$ and $\varphi$ from a punch through test, an assumption of $F_I - \tau$ relation has to be made. This assumption should take into account the problem geometry and the failure mechanism of the rubble. Hence, the derivation of the material properties from the experimental data is not a straightforward task.

First punch through tests were conducted by Leppäranta and Hakala (1992) in the Baltic Sea with a loading platform and concrete blocks. Later more sophisticated equipment for measuring ice rubble strength has been used by e.g. Bruneau et al. (1998) and Croasdale et al. (2001). Heinonen and Määttänen performed a series of experiments during five winters (1998–2003) in the Baltic Sea (Heinonen, 2004; Heinonen and Määttänen, 2000, 2001a,b). In field tests, underwater cameras and measurements on displacements within the keel and keel bottom have been used (Croasdale et al., 2001; Heinonen, 2004), but the possibility to observe the actual failure mechanisms of ice rubble has been rather limited.

To study the failure mechanism of the rubble in more detail, punch through tests in laboratory scale have been performed (Azarnejad and Brown, September, 2001; Azarnejad et al., 1999; Bruneau et al., 1998; Jensen et al., 2001; Lemee and Brown, 2002; Leppäranta and Hakala, 1992). While results from laboratory tests have brought some understanding on the failure mechanisms, the laboratory experiments have also lead to results that partly differ from field tests (Croasdale et al., 2001; Liferov and Bonnemaire, 2005). These differences include the loading rate dependencies of $\tau$ and the failure mode, as first reported by Azarnejad and Brown (2000).

In addition to obtaining the material parameters of the ice rubble, the understanding on failure mechanisms is important for the modeling efforts of ice rubble. The modeling has been performed using soil mechanics models (Ettema and Urroz, 1989), continuum models (Heinonen, 2004; Heinonen and Määttänen, 2001b; Liferov et al., 2002, 2003), discrete models (Polojärvi and Tuhkuri, 2009; Tuhkuri and Polojärvi, 2005) and pseudo-discrete models (Liferov, 2005).

In the work presented in this paper, laboratory scale punch through tests were performed with rubble consisting of plastic blocks. The motivation of using plastic blocks was to simplify the studied phenomena by avoiding bonding due to e.g. freezing and sintering of ice blocks (Ettema and Schaefer, 1986; Kuroiwa, 1961). This type of bonding typically

* Corresponding author. Tel: +358 9 470 23438.
*E-mail address:* arttu.polojarvi@aalto.fi (A. Polojärvi).

0165-232X/$ – see front matter © 2011 Elsevier B.V. All rights reserved.
doi:10.1016/j.coldregions.2011.09.007

occurs in laboratory scale punch through tests if the rubble is left in the basin for a period of time. Even time periods of a few minutes have been reported causing bonding of ice blocks (Ettema and Schaefer, 1986). With the plastic blocks, this type of bonding does not occur.

The experiments were performed in a test basin illustrated in Fig. 1. In the figure, the rubble is not shown for clarity. The tests were pseudo 2D with the indentor platen reaching though the shortest dimension of the basin. The experimental set-up is similar to the laboratory punch through tests with ice rubble described in Azarnejad and Brown (2001). Hence, $F_I-\tau$ relation from their work was adopted for reference. This relation is given by

$$\tau = \frac{F_I^m - F_I^r - F_A}{2bh}, \tag{2}$$

where $F_I^m$ is the maximum force measured during an experiment, $F_I^r$ is the residual force in the end of the indentor stroke and $F_A$ is the inertial force needed to accelerate the rubble. The terms in the previous sentence are those used by Azarnejad and Brown (2001). Further in Eq. (2), $b$ and $h$ are the indentor platen length (see Fig. 1) and the rubble thickness, respectively. Platen length $b$ multiplied by two is used in Eq. (2), as the experiments were pseudo 2D with the platen covering the length of the basin.

Azarnejad and Brown (2001) based Eq. (2) on their indentor force–displacement ($F_I-y_I$) records and observations on the failure mechanism of the rubble. Fig. 2 shows an illustration of a $F_I-y_I$ record from Azarnejad and Brown (2001) with high indentor velocity $v_I$. The maximum force $F_I^m$ was assumed to be due to breakage of the freeze bonds within the rubble. Further, $F_I^r$ was assumed to be the load due to buoyancy of the rubble moving under the indentor after the failure. $F_I^r$ was defined from the measured $F_I$ records using the part where $F_I$ remained approximately constant until the end of the stroke.

Instead of actual punch through tests, Azarnejad and Brown (2001) measured the inertial force $F_A$ from two other types of experiments called here reference experiments. The reference experiments included experiments where the indentor moved into open water and experiments where the indentor moved with a single ice block under it. Similar reference experiments to achieve $F_A$ were also performed here and are in the further text referred to as open water and block experiments, respectively. Even if $F_A$ was called the inertial component by Azarnejad and Brown (2001), it evidently has components other than inertia included in it (Liferov and Bonnemaire, 2005). The experiments performed here showed, that one is due to water in the basin and is here further called hydrodynamic force $F_H$.

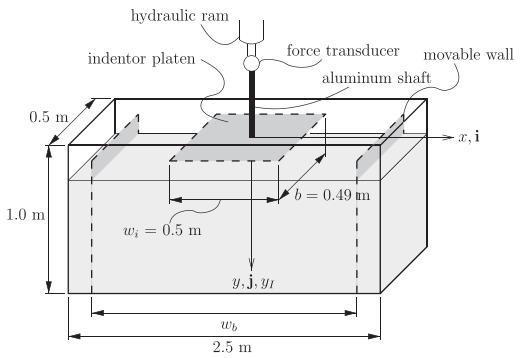


**Fig. 1.** Experimental set up. Direction of the indentor motion $y_I$. The coordinate system $(x,y)$ has its origin in the indentor centroid in its initial position.

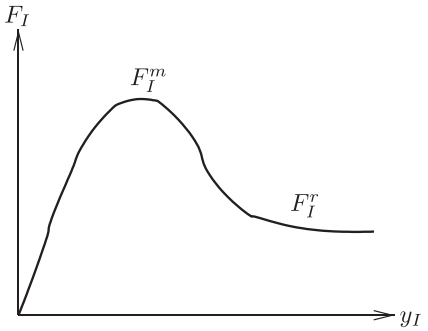


**Fig. 2.** Characteristic indentor force–displacement ($F_I-y_I$) graph from a fast punch through test (Azarnejad and Brown, 2000). The illustration is by the authors of this work.

The main focus of this paper is on the study of a punch through test as a method for measuring rubble properties. Hence, the reference experiments have two-fold significance: (1) they should enable the division of the measured $F_I$ records into factors due to rubble and due to other sources and (2) they should give insight on the applicability of the reference experiments in the interpretation of the punch through tests in general.

The results suggest that analysis of punch through tests based on reference experiments is not straightforward. The division of measured indentor force into components as in Eq. (2) might lead to overestimation of rubble strength with high loading rates. It is shown that the rate dependency may have been overestimated in earlier experiments, i.e. increase in indentor velocity could lead to an overestimation of the ice rubble shear strength. Further, the results suggest that the boundary conditions could affect the results in experiments with high indentor velocities. This could lead to an overestimation of the strength of ice rubble freeze bonds.

The paper is organized as follows. First the experimental set-up is described in detail and then the results are introduced and analyzed. Emphasis in the analysis is on the estimation of rubble strength from punch through tests. After this, the results are discussed and compared with earlier work. The emphasis in the discussion is on the findings that could have affected the results in previous studies. Finally, conclusions are presented.

## 2. Experiments

In this section, the experiments are described in detail. First the experimental set-up is described. After this the experiment types are described in detail and the summary of the testing program is given.

### 2.1. Experimental set-up

The test basin illustrated in Fig. 1 was made of transparent acrylic glass (PMMA) and was supported by a steel frame. The basin dimensions were $2.5\times0.5\times1.0$ m. The indentor platen was $0.5\times0.49\times0.01$ m and made of polyethylene (PE). With the load levels in the experiments, the indentor platen can be considered as rigid. A small gap was left between platen and the basin walls to avoid friction. The platen was attached from its center line to an aluminum shaft. The shaft was attached from its other end to a force transducer further attached to a hydraulic ram. Indentor displacement was measured from the top end of the aluminum shaft using a displacement transducer. The stroke length of the hydraulic ram was 300 mm. The basin had movable walls which enabled to change its width $w_b$. Movable walls were made out of PE and were attached to the basin frame.

**Table 1**
Properties of the rubble blocks.

| Property | Symbol | Unit | Value |
|---|---|---|---|
| Length | – | mm | 90 |
| Width | – | mm | 50 |
| Thickness | – | mm | 20 |
| Material density | $\rho$ | kg m$^{-3}$ | 949 ± 7.834 |
| Friction coefficient | $\mu$ | – | 0.04…0.12 |

The main properties of the rubble blocks are given in Table 1. The rubble consisted of blocks made out of PE. Due to the material and the forces during the experiments, the deformation of individual blocks is expected to be negligible. The blocks were homogeneous in size with a shape of an elongated parallelepiped. Blocks were sawn out of a PE plate of thickness 0.02 m by the supplier of the material. The plate used in manufacturing the blocks had different surface roughness on its opposing faces. The sliding friction coefficient $\mu$ of the blocks was measured for each combination of contacting faces. In the measurements a block was pulled on top of a PE plate with a constant force. From the motion of the block, frictional resistance was derived. A thin layer of water was added to the top of the plate hence the surfaces were wet during a test. The friction was assumed to follow Coulomb friction model. The measured minimum and maximum values of $\mu$ were 0.04 and 0.12 depending on the pair of contacting surfaces.

Most of the experiments were recorded with a video camera. The video recordings were used in analyses of the force records and rubble deformation during experiments.

### 2.2. Description of experiment types

Table 2 gives the summary of the testing program. All experiments were repeated with each set-up and found to be well repeatable as will be shown by the results in Section 3.

In the preparation of an experiment, the rubble blocks were added into the basin until desired rubble thickness $h$ was achieved. After mixing, the rubble was left to settle before conducting an experiment. The time for rubble settling did not affect the results and was only needed to avoid waves in the basin. For another experiment, the rubble was not taken out of the basin but was mixed. This ensured random initial configuration for each experiment.

In the experiments, indentor velocities $v_I$ = 2.5, 5, 10, 20, 30, and 40 mm/s and basin widths 2.3 m and 1.5 m were used. With all $v_I$ used, the indentor velocity remained constant during the indentor stroke as will be shown in Section 3.2. It is believed that with the lowest velocities a case of quasi static loading of the rubble was obtained and the effect of the water could be reliably analyzed. On the other hand, with the highest velocities the hydrodynamic forces were clearly affecting results. Further, with the highest $v_I$ values used, ice rubble has been in earlier laboratory punch through experiments reported to change its failure mode (Azarnejad and Brown, September, 2001). The values of $v_I$ are in the slow regime when compared with the experiments by Azarnejad and Brown (2001), who used indentor velocities up to approximately 120 mm/s. The values of $v_I$ were not chosen to correspond to any full scale ice rubble processes, but to study the experimental method.

In addition to punch through experiments, Table 2 shows the two types of reference experiments: open water and block experiments. The motivation for these was given in Section 1. In the open water and block experiments there was no rubble in the basin and the experiments were performed with the same indentor velocities as the punch though experiments.

In the open water experiments, the indentor with the initial position above the waterline, moved into the basin filled with water only. In the block experiments, a single block with cross sectional size of the indentor and thickness of 0.18 m was placed under the indentor. During an experiment, the block was moving with the indentor. The block was prepared by tightly taping together similar PE blocks as used in the punch through experiments. The block and the indentor platen were initially not in contact. Instead, the block was floating in the basin under the indentor. It is believed that the deformation of the block in the experiments was negligible and the block can be

**Table 2**
Summary of the testing program showing number of conducted experiments. In the table $h$ is the rubble thickness, $w_b$ the basin width, $v_I$ the indentor velocity and N.A. stands for not applicable.

| Test type | $w_b$ [m] | $h$ [m] | $v_I$ [mm/s] | | | | | |
|---|---|---|---|---|---|---|---|---|
| | | | 2.5 | 5 | 10 | 20 | 30 | 40 |
| Punch through | 1.5 | 0.3 | 4 | 4 | 4 | 4 | 4 | 4 |
| | | 0.4 | 4 | 4 | 4 | 4 | 4 | 4 |
| | | 0.5 | 4 | 4 | 4 | 4 | 4 | 4 |
| | 2.3 | 0.3 | 5 | 5 | 5 | 5 | 5 | 5 |
| | | 0.4 | 5 | 5 | 5 | 5 | 5 | 5 |
| | | 0.5 | 5 | 5 | 5 | 5 | 5 | 5 |
| Open water* | 2.3 | N.A. | 3 | 3 | 3 | 3 | 3 | 3 |
| Block* | 2.3 | N.A. | 2 | 2 | 5 | 4 | 4 | 4 |

* Reference experiment.

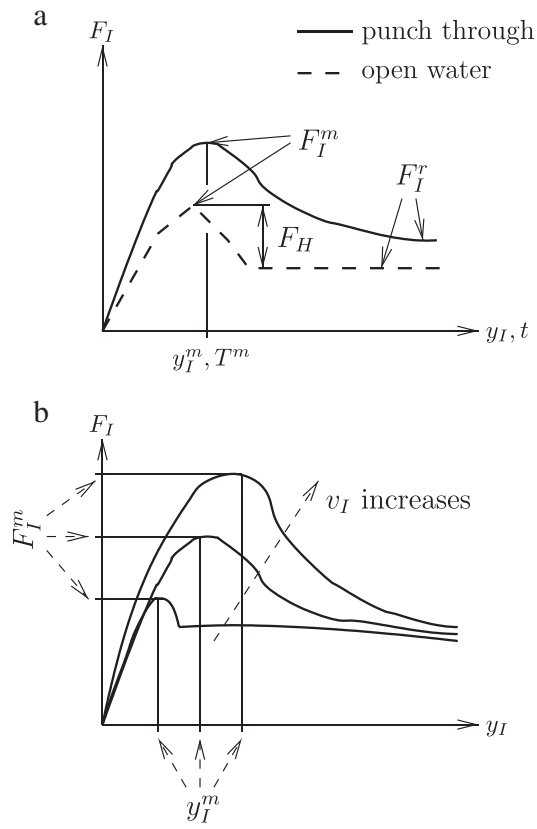


**Fig. 3.** Typical indentor force $F_I$ records (a) and the effect of indentor velocity $v_I$ (b). In (a) $F_I^m$ is the maximum measured indentor force, $F_I^r$ the residual load, and $F_H = F_I^m - F_I^r$ is the hydrodynamic force defined from the results of the open water experiments are illustrated. As (b) shows, increase in $v_I$ caused an increase in $F_I^m$ and the displacement at which $F_I^m$ was reached $y_I^m$ increased in punch through, open water and block experiments.

considered rigid. Further, the same assumption is believed to apply if the block material was changed to ice.

## 3. Results and analysis

In this section, the indentor force–displacement ($F_I - y_I$) and the indentor force–time ($F_I - t$) records from the experiments are described and analyzed. Fig. 3 a illustrates typical $F_I$ records from a punch through and an open water experiment. In addition, the figure shows how the terms in Eq. (2) were derived from the $F_I$ records.

As Fig. 3 a shows, $F_I^m$ refers to the maximum measured indentor force and $F_I^r$ to the force at the end of an experiment. $F_I^m$ occurs at time $T^m$ and with indentor displacement $y_I^m$ as indicated. The hydrodynamic force $F_H$ was derived from $F_I$ records of the open water experiments as $F_H = F_I^m - F_I^r$. The derivation of the inertial force $F_A$ in Eq. (2) was similar to $F_H$ with the exception, that $F_I$ records of block experiments were used.

As illustrated in Fig. 3 b, the indentor velocity $v_I$ changed the $F_I$ records. An increase in $v_I$ caused an increase in $F_I^m$ and in $y_I^m$. However, $T^m$ decreased with increasing $v_I$. This occurred in all punch through, open water and block experiments with increasing $v_I$. As will be shown below, changes in $F_I$ records with $v_I$ are largely due to hydrodynamic forces.

In the following analysis, the mean force records and values are used. These were derived using $F_I$ records from all of the experiments with the same set up. The mean force records in the text are indicated by bar symbol, e.g. $\bar{F}_I$ records refer to $F_I$ records averaged over the experiments with the same set up.

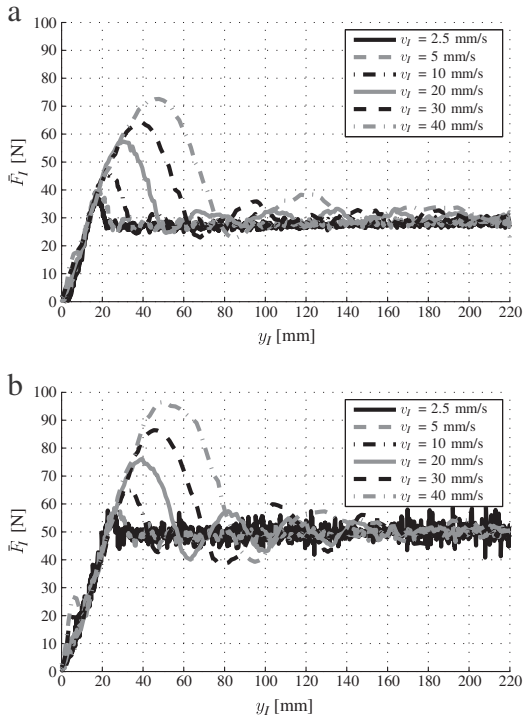


**Fig. 4.** Mean indentor force-displacement ($\bar{F}_I - y_I$) records from (a) open water and (b) block tests with all values of indentor velocity $v_I$.

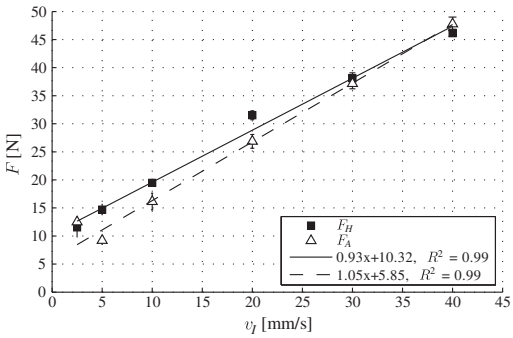


**Fig. 5.** The hydrodynamic force $F_H$ and inertial force $F_A$ as function of indentor velocity $v_I$.

### 3.1. Hydrodynamic and inertial force

As shown in Fig. 4, the open water and block experiments resulted to $F_I - y_I$ records with very similar shape close to the maximum indentor load $F_I^m$ with all $v_I$. The difference in the value of $F_I^m$ in open water and block experiments was approximately equal to the block buoyancy $F_B^b$. In both experiments the residual force $F_I^r$ was due to buoyancy; in open water experiments due to the indentor buoyancy $F_I^b$ and in block experiments due to the sum of indentor buoyancy and block buoyancy,

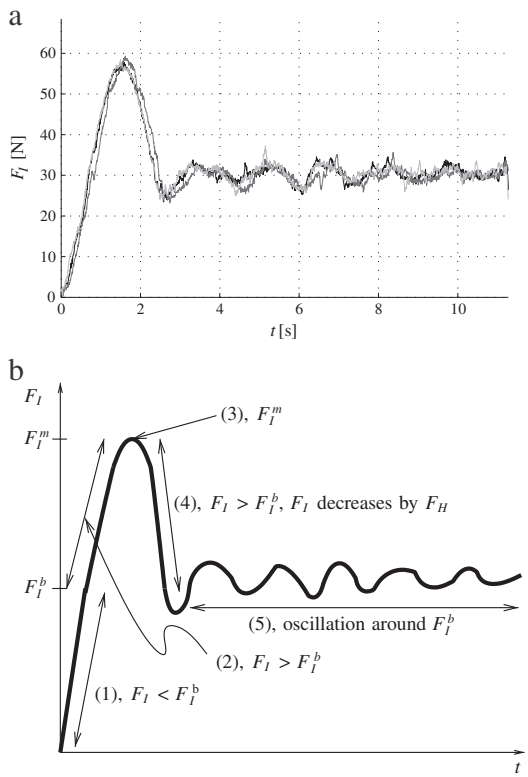


**Fig. 6.** The division of $F_I - t$ records from open water experiments into five parts (1)–(5): (a) measured $F_I - t$ from three open water experiment with $v_I = 20$ mm/s and (b) division of $F_I - t$ records into five parts. Further, (b) shows the definition for each part. The observations related to the parts (1)–(5) are described in Fig. 6.

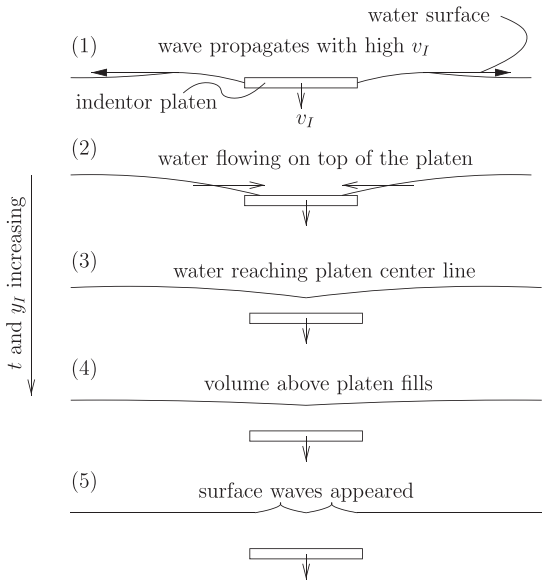


**Fig. 7.** Observations from the open water experiments divided into parts (1)–(5). In the illustrations indentor platen is moving downwards with velocity $v_I$. The $F_I-t$ record with the same parts indicated are given in Fig. 6 b.

$F_I^b + F_B^b$. The transient peak in the beginning ($y_I \approx 5$ mm) of the block experiments with high $v_I$ seen in Fig. 4 was likely due to block inertia.

Before analyzing the $F_I$ records in more detail, the values of hydrodynamic force $F_H$ obtained from the open water experiments and inertial force $F_A$ obtained from the block experiments are shown in Fig. 5 as a function of indentor velocity $v_I$. In addition, the figure shows linear fits for both data sets. It can be seen, that the values of $F_A$ and $F_H$ somewhat differ with low $v_I$ and the rate $\partial F_A/\partial v_I$ is slightly higher than $\partial F_H/\partial v_I$. Anyhow, as will be shown in next section, these differences in force values are small when compared to the results of punch through experiments.

The similar shapes of $F_I$ records close to the maximum indentor force $F_I^m$ suggest that the increase in $F_I^m$ with increasing $v_I$ was likely due to same reason in the open water and the block experiments. For clarity, the $F_I$ records from open water experiments and $F_H$ are considered here but the same analysis applies for block experiments and $F_A$.

For the analysis of $F_H$, Fig. 6 a and b shows $F_I-t$ records from three open water experiments and an illustration of the same data, respectively. Fig. 6 b shows that the division of $F_I-t$ graph is into five parts.

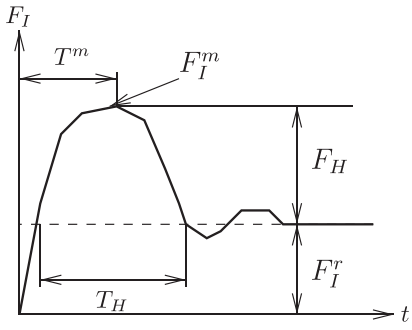


**Fig. 8.** Time interval $T^m$ to maximum load $F_I^m$ in open water experiments. Also the time interval $T_H$ during which $F_H$ occurs is shown.

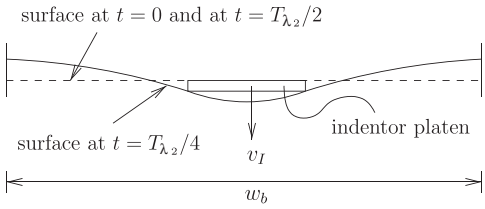


**Fig. 9.** The second mode of stationary wave in the basin with width $w_b$. In the figure the indentor excites the wave at $t=0$. During $t=T_{\lambda_2}/4 \ldots T_{\lambda_2}/2$ water mass under the indentor moves upwards.

To further describe parts (1)–(5), the observations made during experiments are related to them by a sequence of illustrations in Fig. 7. In Fig. 6 a, the data is from experiments with $v_I = 20$ mm/s, but the division of $F_I-t$ records in Fig. 6 b applies for all $v_I$. It should be noticed, that the same division of $F_I$ records applies to block experiment results. The only exception is that block buoyancy $F_B^b$ has to be taken account when defining parts (1)–(5) in Fig. 6 b.

As Figs. 6 and 7 show, during (1) $F_I$ increases due to indentor buoyancy as it starts its entry to the water. The observations on experiments with high $v_I$ showed, that a small surface wave could start propagating during (1) as shown in Fig. 7. When $F_I < F_I^b$, the rate $\partial F_I/\partial y_I$ increased only slightly with $v_I$, indicating that the load increase was mostly due to buoyancy during (1) with all $v_I$.

During stage (2), the rate $\partial F_I/\partial t$ decreased but $F_I$ still increased with all $v_I$. The observations showed, that during (2) the water flowed on top of the indentor towards its center line. Hence, the platen was under the initial water surface, but not instantly covered by water. As $F_I^m$ at (3) was reached, the water had reached indentor center line. After this, during (4), $F_I$ decreased towards its residual value and the volume above indentor was filling with water. As $F_I \approx F_I^b$ at the beginning of (5), surface waves with short wave length appeared on top of the indentor if $v_I$ was high.

The maximum force $F_I^m$ in open water and block experiments was not due stationary waves in the basin. To show this, the time to maximum load $T^m$ illustrated in Fig. 8 was derived from the data. Similarly to $T^m$, time interval $T_B^m$ to reach $F_I^m$ in block experiments was derived. $T^m$ and $T_B^m$ were compared to the periods of the stationary waves in the basin $T_{\lambda_n}$. The solution for $T_{\lambda_n}$ given in e.g. Faltinsen (1990) is

$$T_{\lambda_n} = \sqrt{\frac{2\pi\lambda_n}{g}\left[\tanh\left(\frac{2\pi}{\lambda_n}h_{W\cdot}\right)\right]^{-1}}, \tag{3}$$

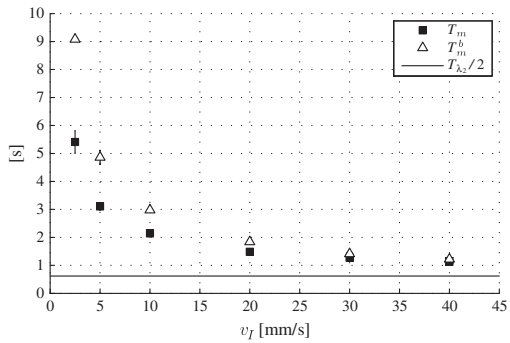


**Fig. 10.** Time intervals $T^m$ and $T_B^m$ to maximum load from the open water and block experiments. In addition the half period $T_{\lambda_2}/2$ of the second mode surface wave is shown (see Eq. (3)).

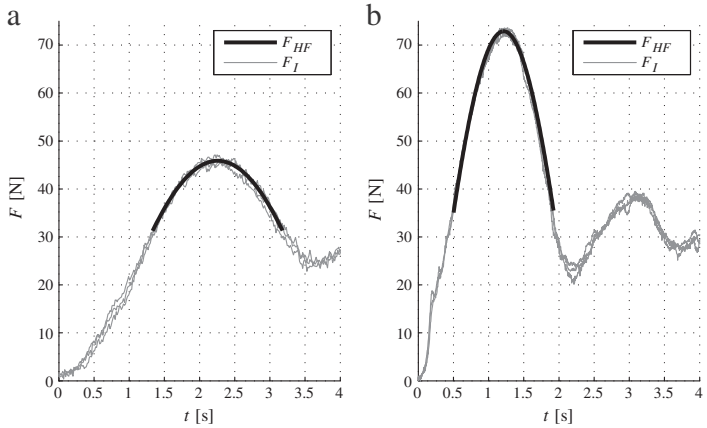


**Fig. 11.** Fitting function $f_{HF}$ given by MATLAB (see Eq. (4)) shown on top of the original data from three open water experiments: In (a) $v_I = 10$ mm/s and in (b) $v_I = 40$ mm/s. In both cases $f_{HF}$ gives a good estimate for $T_H$.

where $\lambda_n$ is the wave length of mode $n$, $g$ the gravitational acceleration, and $h_W$ the water depth. The stationary waves have relation between $\lambda_n$ and basin width: $\lambda_n = 2w_b/n$.

Based on observations, the second mode ($n=2$) as illustrated in Fig. 9 with $\lambda_2 = w_b$ m is of interest. As illustrated in the figure, from $T_{\lambda_2}/4 < t < T_{\lambda_2}/2$ the water mass under the indentor is moving towards it. Hence, if $F_H$ was due to stationary wave, it should occur with $t < T_{\lambda_2}/2$. By substitution of $w_b = 2.3$ m, $h_W = 0.6$ m, $g = 9.81$ ms$^{-2}$ into Eq. (3) value $t < T_{\lambda_2}/2 < 0.63$ s is achieved. It should be noticed, that $T_{\lambda_2}$ decreases with increase in $h_W$ and water depth in the basin was always more than 0.6 m i.e. $T_{\lambda_2}/2$ in the experiments would have been even shorter.

Time periods $T^m$ and $T_B^m$ are shown against $v_I$ in Fig. 10 a with $T_{\lambda_2}/2$. The figure shows, that $T^m$ and $T_B^m$ are not constant, but decrease with $v_I$. If the surface waves were to cause $F_H$ or $F_A$, this would not be expected. Further, $T^m$ ($T_B^m$) is too long for a wave to cause $F_H$ ($F_A$). Hence, the water mass moving towards the indentor due to stationary wave does not cause $F_H$ (see Fig. 9). Anyhow, the wave that started to propagate horizontally away from the indentor at (1) in Fig. 7 could partly lead to instantaneous $F_H$ in fast experiments. In case they reflect back from the basin walls, they could help the water flow on top of the indentor.

As will be shown in the next section, the $F_I$ records from the punch through tests showed a peak corresponding to $F_H$. To compare the $F_I - t$ records from the open water and punch through experiments, a least squares fit on the open water experiments data was defined. For the fit, first the time interval $T_H$ of $F_I > F_I^r$ shown in Fig. 8 was derived from $F_I - t$ records of open water experiments. As the figure shows, $T_H$ is the time interval during which $F_H$ occurs in the open water experiments.

For period $T_H$ with each $v_I$ a curve was fitted using MATLAB® and fminsearch function (MATLAB, 2009). Here, a sinusoidal fit was chosen and MATLAB was used to find constants $C_1$, $C_2$ and $C_3$ for function

$$f_{HF}(t) = C_1 \sin\left(\frac{2\pi t}{C_2}\right) + C_3. \tag{4}$$

MATLAB's fminsearch solves constants $C_I$ by finding the least squares fit based on the data. At the start of the iteration an initial guess for the constants has to be given. Here initial guesses $C_1 = F_I^m - F_I^r$, $C_2 = 2T_H$ and $C_3 = F_I^r$ were used. Fig. 11 a and b shows the fits on top of the original data from the open water experiments with two values $v_I$.

For further use, $f_{HF}$ is translated for each experiment. The idea of the translation is illustrated in Fig. 12. Briefly, translation aligns $f_{HF}$ with the maximum indentor force $F_{I,j}^m$ of experiment $j$ and for the comparison of punch through and open water experiments. For experiment $j$, the fit after translation is

$$F_{HF}(t) = f_{HF}\left(t + \left[T_j^m - T^m\right]\right) + \left[F_{I,j}^m - \max(f_{HF})\right], \tag{5}$$

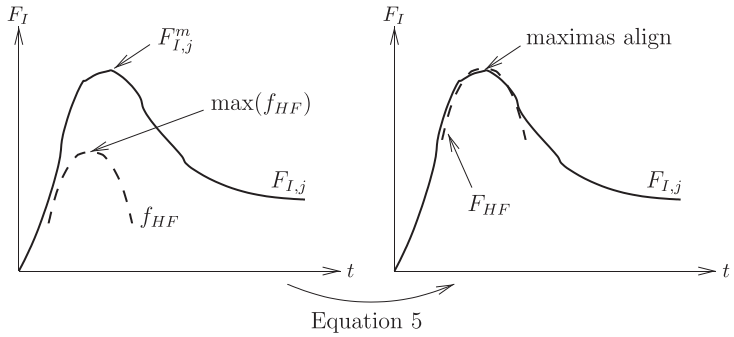


**Fig. 12.** Eq. (5) translating $f_{HF}$ to $F_{HF}$ according with $F_I - t$ record of experiment $j$ ($F_I$,$j$). The load record $F_{I,j}$ does not move due to Eq. (**5**).

where $T^m$ and $T_j^m$ are the time instants of maximum indentor forces $F_I^m$ and $F_{I,j}^m$ in open water and punch through experiment $j$, respectively.

### 3.2. Force records in punch through experiments

Fig. 13 shows the indentor force $F_I$ and indentor displacement $y_I$ from four repeated slow punch through experiments with basin width $w_b = 1.5$ m and rubble thickness $h = 0.5$ m. As illustrated by the $F_I$ records, the experiments were well repeatable. Indentor displacement $y_I$ records show that the indentor velocity $v_I$ remained constant during the experiments. The data in the figures was used to derive the mean indentor force record $\bar{F}_I$ for $w_b = 1.5$ m shown in Fig. 14 a and b. Fig. 14 a shows the mean indentor force displacement ($\bar{F}_I - y_I$) records from the punch through experiments with both $w_b$. As shown by the figure, both $w_b$ yielded to similar $F_I - y_I$ records.

In the beginning of an experiment, $\bar{F}_I$ starts to increase due to resistance and buoyancy of the rubble as shown in Fig. 14 a. It should be noticed that, due to rubble buoyancy, $F_I$ starts to increase before the indentor begins to submerge. With increasing $y_I$, first the rate $\partial \bar{F}_I / \partial y_I$ changes and then $\bar{F}_I$ reaches its maximum $\bar{F}_I^m$.

The change in $\partial \bar{F}_I / \partial y_I$ and $\bar{F}_I^m$ is explained by the results from the open water experiments. For this, $\bar{F}_I - t$ records close to the peak for the same experiments are shown in Fig. 14 b. In addition to $\bar{F}$, the figure shows the fit $F_{HF}$ (see Fig. 12) from the open water experiments with the same indentor velocity $v_I$.

As Fig. 14 b shows, the peak giving $\bar{F}_I^m$ matches with $T_H$ shown in Fig. 8. This suggests that maximum indentor force $\bar{F}_I^m$ is related to the hydrodynamic force $F_H$. The change in the rate $\partial \bar{F}_I / \partial t$ (and thus in $\partial \bar{F}_I / \partial y_I$ in Fig. 14 a at $y_I \approx 50$ mm) occurred due to increase in buoyant load as the indentor started its entry into the water.

After the peak related to $F_H$ in Fig. 14 a, $\bar{F}_I$ corresponds to the rubble resistance and to the combined load of the rubble and indentor platen buoyancies. It can be noticed, that $\bar{F}_I$ slowly decreases until

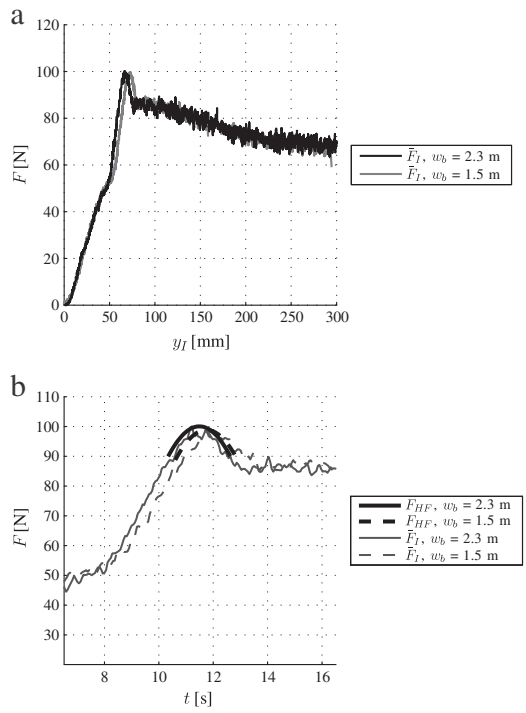


**Fig. 14.** Mean indentor force $F_I$ records from punch through experiments with $v_I = 5$ mm/s, $h = 0.5$ m, and with both basin widths $w_b$: (a) $F_I - y_I$ records and (b) $F_I - t$ records close to maximum indentor force with the fit $F_{HF}$ from the open water experiments (see Fig. 12). Number of experiments for each set up shown is given in Table 2.

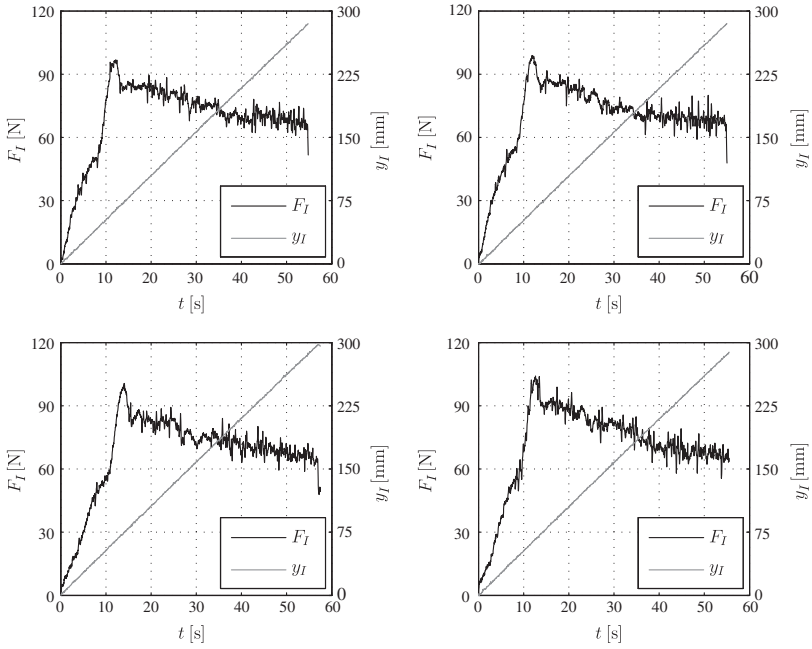


**Fig. 13.** The measured indentor force $F_I$ and displacement $y_I$ plotted against time $t$ from four repeated experiments with $v_I = 5$ mm/s, $h = 0.5$ m and $w_b = 1.5$ m. The records shown in the figures were used to derive the mean indentor force $F_I$ record shown in Fig. 14.

the end of the experiment. Hence, no constant residual force $F_I^r$ was measured in the experiments.

As was already illustrated in Fig. 3 b, the $F_I$ records changed with indentor velocity $v_I$. Fig. 15 shows the measured $F_I$ and $y_I$ from four repeated fast ($v_I = 40$ mm/s) punch through experiments with basin width $w_b = 1.5$ m and rubble thickness $h = 0.5$ m. The fast experiments were well repeatable, and the indentor velocity stayed constant during each experiment as shown by the figures. The data in the figures was used to derive the mean indentor force $\bar{F}_I$ record for $w_b = 1.5$ m shown together with the $\bar{F}_I$ record for $w_b = 2.3$ m in Fig. 16 a. The basin width $w_b$ did not have major effect on the $\bar{F}_I - y_I$ records.

Fig. 16 a shows that $\bar{F}_I$ increased with high rate $\partial \bar{F}_I / \partial y_I$ from the beginning of the experiment. The rate $\partial \bar{F}_I / \partial y_I$ in the fast experiments was higher than in their slow counterparts (see Fig. 14 a). Close to the maximum force $F_I^m$, the shape of the $F_I$ records again corresponded to $F_{HF}$ obtained from the open water experiments with same indentor velocity $v_I$. This is seen from Fig. 16 b, which shows $\bar{F}_I - t$ records close to $\bar{F}_I^m$ with the fit $F_{HF}$ (see Fig. 12). As observed from the figure, $F_I$ continued to decrease fast even after $F_{HF}$ unlike in the slow experiments (see Fig. 14 b).

The maximum indentor force $F_I^m$ increased with $v_I$ as shown by Fig. 17 a and b. In addition to $F_I^m$ from punch through experiments, the figure shows $F_I^m$ from the open water and block experiments. Further, Table 3 shows the mean values of $F_I^m$ for all experimental set ups with their standard deviations. As shown by the table, the standard deviations were relatively small indicating good repeatability of the experiments.

As Fig. 17 a and b show, in punch through experiments, $\partial F_I^m / \partial v_I$ was clearly higher than in open water and block experiments. The difference between rates $\partial F_I^m / \partial v_I$ in open water and block experiments was small, when compared to the rate $\partial F_I^m / \partial v_I$ from punch through experiments.

The results in Fig. 17 a and b show some increase in $\partial F_I^m / \partial v_I$ with $h$, but the increase is small when compared to total change in $F_I^m$ with $v_I$. Further, the basin width $w_b$ did not have major effect on maximum

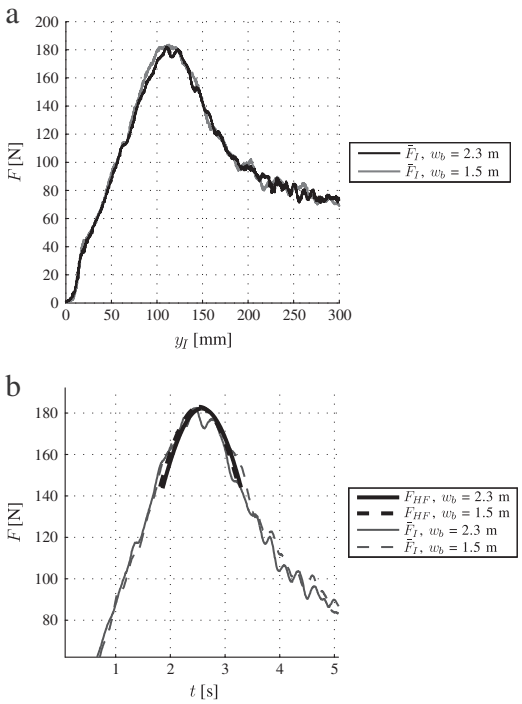


**Fig. 16.** Mean indentor force $\bar{F}_I$ records from punch through experiments with $v_I = 40$ mm/s, $h = 0.5$ m, and with both basin widths $w_b$: (a) $\bar{F}_I - y_I$ records and (b) $\bar{F}_I - t$ records close to maximum indentor force with the fit $F_{HF}$ from the open water experiments (see Fig. 12). Number of experiments for each set up shown is given in Table 2.

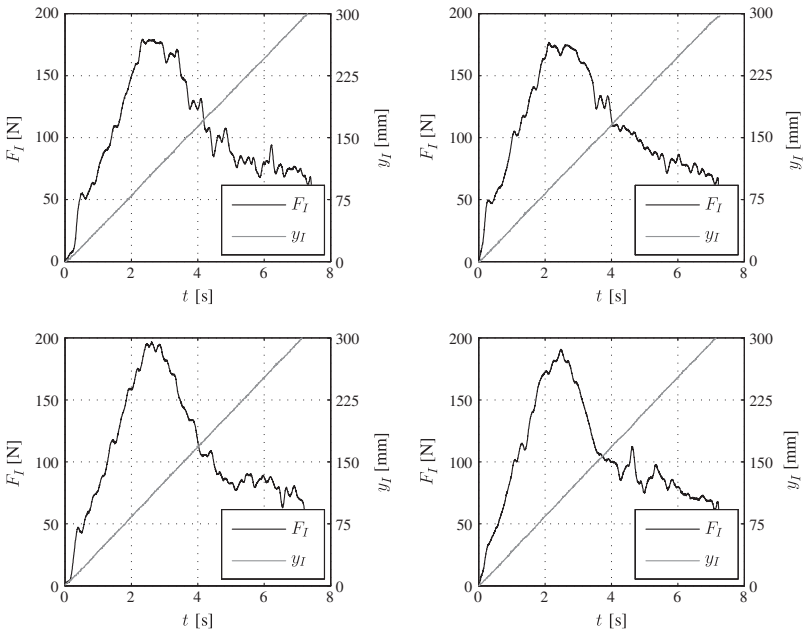


**Fig. 15.** The measured indentor force $F_I$ and displacement $y_I$ plotted against time $t$ from four repeated experiments with $v_I = 40$ mm/s, $h = 0.5$ m and $w_b = 1.5$ m. The records shown in the figures were used to derive the mean indentor force $\bar{F}_I$ record shown in Fig. 16.

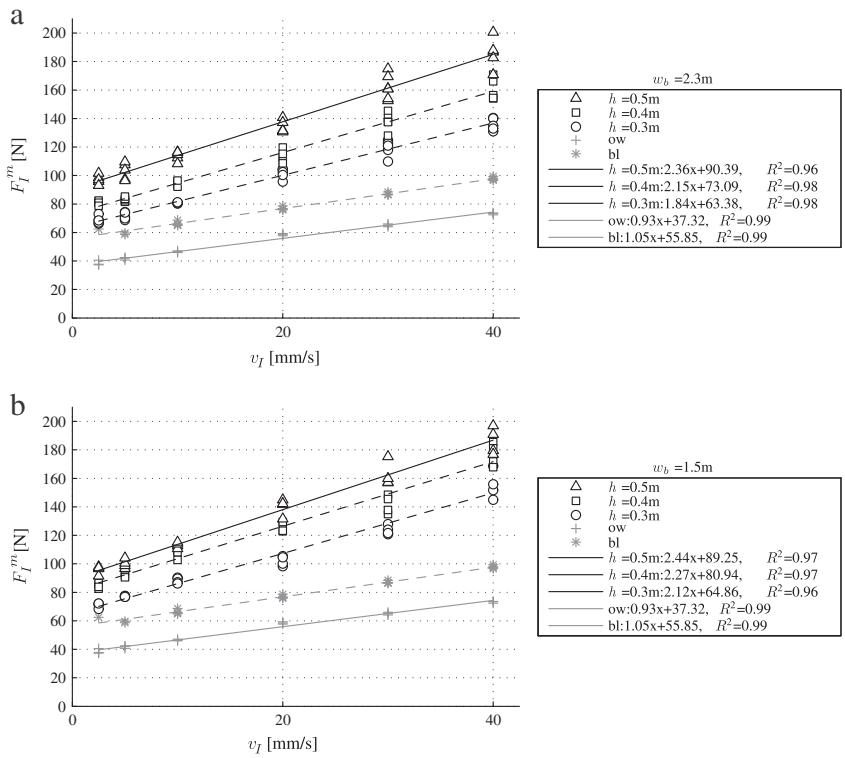


**Fig. 17.** Maximum indentor force $F_I^m$ from punch through experiments with basin widths (a) $w_b = 2.3$ m and (b) $w_b = 1.5$ m. In addition, $F_I^m$ from the open water (ow) and block experiments (bl) are shown.

force $F_I^m$. Accounting all experimental set ups, on average 5% higher values of $F_I^m$ were measured with $w_b = 1.5$ m.

### 3.3. Indentor velocity induced effects in experiments

#### 3.3.1. Deformation patterns and velocity

The rubble behavior in the experiments was affected by the experimental set up and hydrodynamic forces. To show this, the $F_I$ records from a slow and fast experiment and sequences of snapshots from the same two experiments are shown in Figs. 18 and 19, respectively. The snapshots in Fig. 19 show the experiments at four different indentor displacements $y_I$. Further in the snapshots, the typical deformation patterns of the rubble are described.

Before discussing the deformation of the rubble in more detail, the rubble mass moving down with the indentor until the end of the experiment is considered. This mass is indicated in Fig. 19 (1b) and (2a) for the fast and the slow experiment, respectively, and has a shape of upward opening trapezoid. This trapezoidal volume evolved early in the experiment from a mass with a shape of an upward opening wedge.

As observed from Fig. 19, the rubble mass moving down with the indentor remained similar irrespective of $v_I$. In the end of an experiment, major part of $F_I$ is expected to consist of rubble and indentor buoyancies. The similarity of the rubble mass moving down with the indentor in slow and fast experiment explains the similarity of the indentor load $F_I$ at the end of the experiments (see Fig. 18).

At (1a) and (1b) in Figs. 18 and 19, the indentor has just submerged in both experiments. The slow experiment reached maximum indentor load $F_I^m$ at this point of the experiment as (1a) in Fig. 18 a shows. As in open water experiments (see (2) in Fig. 7), in slow experiments $F_I^m$ occurred after indentor submergence, but at the stage, when the indentor platen was not yet totally covered by water.

As already mentioned, in the fast experiments $F_I^m$ occurred at higher indentor displacement than in the slow experiments. The instance of $F_I^m$ in the fast experiment is indicated by (2b) in Fig. 18 b and shown in the snapshot in Fig. 19 (2b). The occurrence of $F_I^m$ in fast experiments was accompanied with rapid flow of water through the rubble mass towards the indentor center line. However, at (2b) in Fig. 19 the rubble mass restricts the flow of water on top of the indentor. Hence the force needed to enable the flow is higher than in the open water experiments. Simultaneously, the movement of the blocks over the indentor is obstructed by the indentor platen. This can be seen from (2b) in Fig. 19, where virtually no rubble blocks are observed moving over the indentor with the water flow. The indentor platen obstructing the movement of rubble blocks with the

**Table 3**
Mean values of maximum values indentor force $F_I^m$ with their standard deviations from the punch through experiments. Data from the experiments with all rubble thicknesses $h$ and indentor velocities $v_I$ and both basin widths $w_b$ used is given.

| $w_b$ [m] | $h$ [m] | $v_I$ [mm/s] | | | | | |
|---|---|---|---|---|---|---|---|
| | | 2.5 | 5 | 10 | 20 | 30 | 40 |
| 1.5 | 0.3 | 71 ± 2 | 77 ± 0 | 88 ± 2 | 102 ± 3 | 124 ± 3 | 155 ± 10 |
| | 0.4 | 85 ± 2 | 94 ± 3 | 107 ± 3 | 126 ± 3 | 142 ± 6 | 177 ± 8 |
| | 0.5 | 96 ± 3 | 100 ± 3 | 113 ± 2 | 140 ± 6 | 162 ± 9 | 186 ± 9 |
| 2.3 | 0.3 | 69 ± 3 | 72 ± 2 | 81 ± 0 | 101 ± 4 | 119 ± 6 | 136 ± 4 |
| | 0.4 | 81 ± 1 | 83 ± 1 | 94 ± 2 | 113 ± 4 | 138 ± 6 | 160 ± 8 |
| | 0.5 | 97 ± 3 | 103 ± 6 | 114 ± 3 | 134 ± 4 | 162 ± 9 | 186 ± 11 |

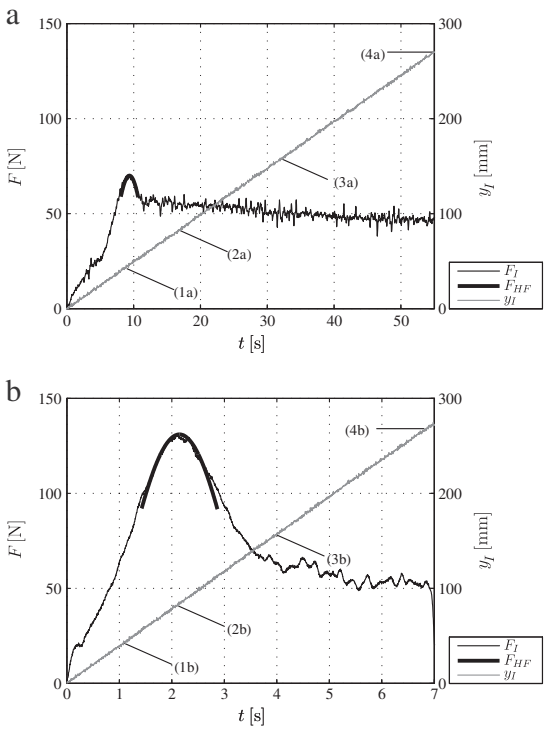


**Fig. 18.** The $F_I$ records for the experiments shown in the sequence of snapshots in Fig. 19 with indentor velocities (a) $v_I = 5$ mm/s and (b) $v_I = 40$ mm/s. The $F_I$ records are from the experiments with rubble thickness $h = 0.3$ m and basin width $w_b = 2.3$ m. Markers in the figures correspond to the snapshots in Fig. 19. In addition, fit $F_{HF}$ from the open water experiments (see Fig. 12) and the indentor displacement $y_I$ are shown.

water can lead to an increase in $F_I^m$, not only due the rubble properties, but also due to the set up of the experiment.

After (2b) in the fast experiment, the rubble started to move over indentor as indicated by arrows marked with (A) in Fig. 19 (3b). This movement of rubble started immediately after $F_I^m$ was reached and continued during the fast decrease in $F_I$ records between (2b) and (3b) in Fig. 18 b. By stage (3b) in Figs. 18 and 19, movement of the rubble upwards indicated by arrows marked with (B) had started. As observed from Fig. 19 (3a), similar movement occurred also in the slow experiment, but was considerably slower and involved less rubble.

The rubble motion in fast experiment as indicated in Fig. 19 (3b) inevitably leads to a change in rubble configuration in the vicinity of the indentor. This movement depends on the experimental set up, as the movement is enabled by the indentor platen moving down i.e. the boundary conditions for the rubble change during the experiment. Once the rubble moves towards the platen center line, the flow of water on top of the indentor becomes less restricted. This likely partly causes the fast decrease in $F_I$ between (2b) and (3b) fast experiments seen in Fig. 18 b.

With an increase in indentor velocity $v_I$ an increase in the rubble mass moving on top of the indentor occurred as comparison of Fig. 19 (4a) and (4b) shows. This is again due to flow of water enforced by higher $v_I$.

### 3.3.2. Other velocity related effects

The above discussion on deformation patterns and their relation to indentor force $F_I$ records suggest that the experimental set up effects the results: the drop in the indentor force from $F_I^m$ to residual value $F_I^r$ is likely related to the change in boundary conditions for the rubble during the experiment (see (3b) in Fig. 19) rather than material properties of the rubble. However, it is clear that with fast loading rates, $F_I$ records and values of maximum indentor force $F_I^m$ could also increase due to other reasons. The reasons considered here are: (1) inertial force of the accelerating rubble mass, (2) the permeability of the rubble mass, and (3) the force $F_P$ induced by pore pressure within the deforming rubble.

The inertial force of the accelerating rubble mass can be considered as follows. If inertia had a considerable effect on $F_I^m$, an increase in $h$ would be expected to lead to an increase in $\partial F_I^m/\partial v_I$ as the rubble mass increases with $h$. As was already mentioned, the change in rate $\partial F_I^m/\partial v_I$ with $h$ was small when compared to the total change in $F_I^m$ with $v_I$ (see Fig. 17). Hence it appears, that the inertia does not have a major effect on the value of $F_I^m$. It should also be noticed that in the block experiments, the inertia of the block had virtually no effect on $F_I^m$ (see Section 3.1).

The permeability of the rubble evidently affects the load. In addition to its relation to the force induced by pore pressure $F_P$, it has an effect on the flow of water through the rubble mass into the volume on top of the indentor. As was observed from Fig. 19 (2b), this flow was restricted by the porous rubble mass as $F_I^m$ was reached in fast experiments. After $F_I^m$ was reached, rubble blocks moved with the water flow above the indentor platen as was shown in Fig. 19 (3b). This movement of rubble likely causes a change in the permeability of the rubble mass in the vicinity of the indentor. Hence, the effect of permeability is likely also related to the experimental set up.

Whether the force due to pore pressure, $F_P$, affects $F_I$ is difficult to estimate. If it does, it is likely related to experimental set up in similar way as rubble permeability. Anyhow, if $F_P$ does increase the maximum indentor force $F_I^m$, its effect would be expected to increase with rubble thickness $h$. As in the case of inertia, the relatively small change in the rate $\partial F_I^m/\partial v_I$ with $h$ compared to the total change in $F_I^m$ with $v_I$ indicates, that $F_P$ had no major effect on $F_I^m$ in the experiments.

### 3.4. Estimation of rubble shear strength $\tau$

The rubble shear strength $\tau$ defined in Eq. (2) can be derived from the indentor force $F_I$ records of the experiments. It should be noticed, that in these experiments, no peak load corresponding to breakage of a network of cohesive bonds was observed. Instead, the peak observed in $F_I$ records was related to the hydrodynamic force $F_H$ (see Figs. 14 and 16). Rationale for deriving $\tau$ is thus to investigate the relation of $F_I$ records and $\tau$ given in Eq. (2).

Derivation of maximum force $F_I^m$ (see Eq. (2)) from $F_I$ records of the experiments was presented above. Here $F_H$ was used instead of $F_A$ in Eq. (2). This was done as the difference in $F_A$ obtained from block experiments and $F_H$ obtained from open water experiments (see Fig. 5) was negligible when compared to difference in $F_I^m$ and $F_I^r$ in punch through experiments with high indentor velocities $v_I$: with $v_I > 10$ mm/s, the difference in $F_A$ and $F_H$ was less than 5% when compared to the difference in $F_I^m$ and $F_I^r$ from all experiments. For the residual force $F_I^r$ in punch through experiments, the mean value of $F_I$ after the fast decrease in $F_I$ was used.

Eq. (2) yielded rubble shear strength $\tau$ values on the range of 30… 150 Pa with $\tau$ increasing linearly with indentor velocity $v_I$. With low $v_I$, $F_I$ after the peak (which is related to hydrodynamic load $F_H$) corresponded to the rubble resistance and the combined load due to rubble and indentor buoyancies. As illustrated by Fig. 20 a, once $F_I = F_I^m - F_H$ is reached after the peak, $F_I$ gradually decreases towards its residual value $F_I^r$.

The rubble shear strength $\tau$, as defined in Eq. (2), corresponds to this decrease, or the difference between $F_I^m - F_H$ and $F_I^r$. The problem with this definition of rubble shear strength $\tau$ is that the load levels $F_I^m - F_H$ and $F_I^r$ are not measured for the same experimental set up. The load $F_I^m - F_H$ is obtained in the beginning of an experiment while the load

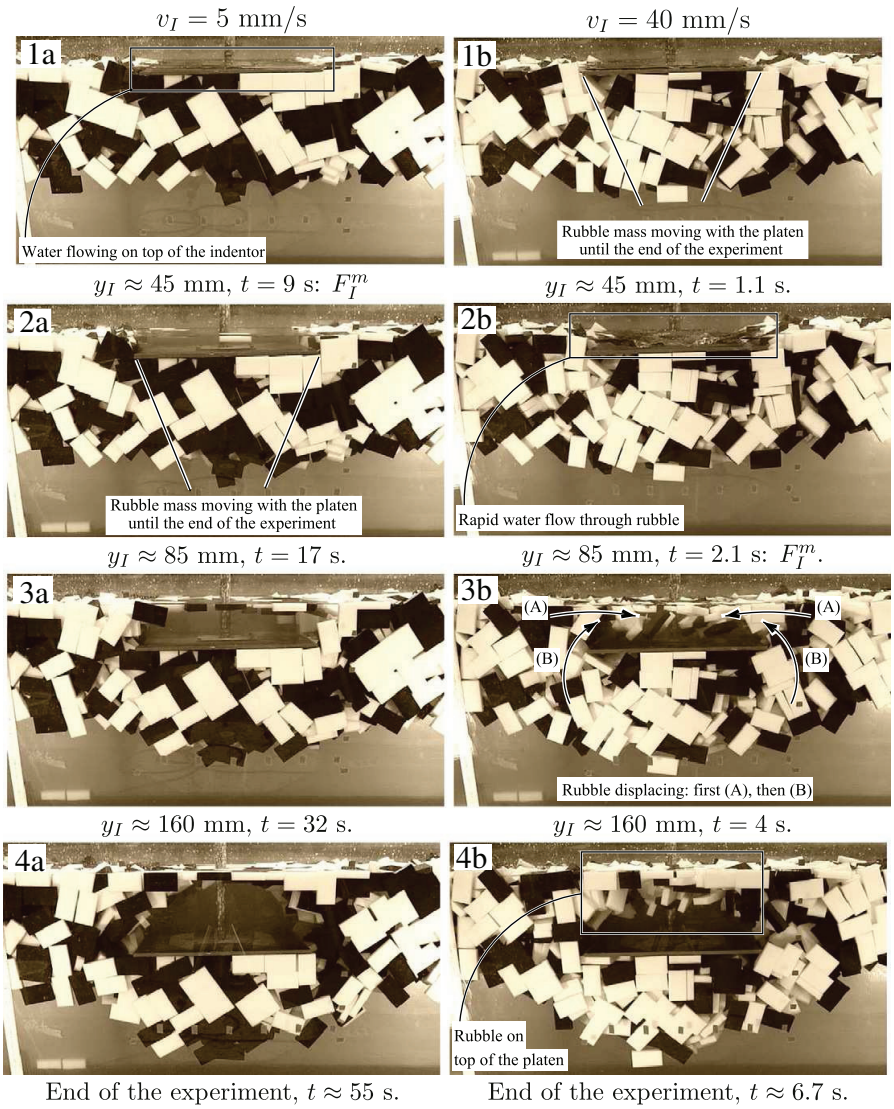


**Fig. 19.** Sequences of snapshots from a punch through experiments with $v_I = 5$ mm/s (left column) and $v_I = 40$ mm/s (right column) with four different indentor displacements $y_I$. In the experiments shown, rubble thickness $h = 0.3$ m and basin width $w_b = 2.3$ m. Indentor force $F_I$ records from the same experiments are given in Fig. 18.

$F_I^r$ is measured at a much later stage, where the amount of rubble below the indentor has decreased, as shown in Fig. 19. In other words, the rubble thickness $h$ in Eq. (2) cannot be unambiguously defined, and the value of rubble shear strength $\tau$ is related to a change in the experimental set up. Disturbingly, this means also that the value of $\tau$ depends on how far the indentor moves (see Fig. 20).

The features described above are much more pronounced in high speed tests than in slow speed tests. In high speed tests the change in rubble configuration during an experiment is more remarkable (see Fig. 19), the hydrodynamic load component $F_H$ is higher, and an even less clear residual force level $F_I^r$ was observed (see Fig. 20). As the hydrodynamic force $F_H$ is obtained from the reference experiments with no rubble, the more the rubble effects the water flow, the more $F_H$ may differ from the hydrodynamical effects during a punch through test.

In these experiments, the rubble shear strength $\tau$, as defined in Eq. (2), was observed to increase with velocity. This result is similar with laboratory experiments with ice rubble. However, with all the above mentioned problems in the definition of $\tau$ and the strong effect of velocity on the behavior of rubble and water, it is possible that the measured loading rate dependency of $\tau$ is caused by the test set up and not by the rubble.

## 4. Discussion

### 4.1. Comparison to earlier laboratory experiments

The shear strength values of the rubble were compared to those from the earlier laboratory scale punch through on ice rubble by Azarnejad and Brown (2001). In their work, series of experiments were performed

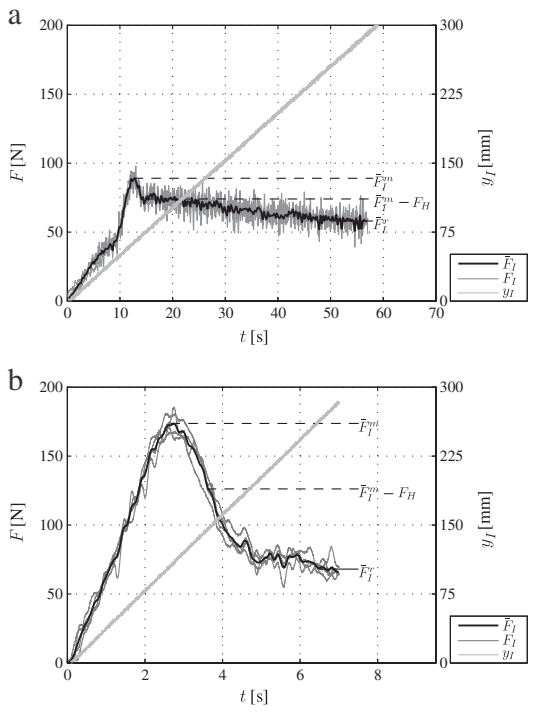


**Fig. 20.** Mean indentor force $\bar{F}_I - t$ records showing the mean maximum indentor load $\bar{F}_I^m$, indentor load after the peak related to $F_H$ ($\bar{F}_I^m - F_H$) and residual load $\bar{F}_I^r$ in experiments with (a) $v_I = 5$ mm/s and (b) $v_I = 40$ mm/s. In all experiments shown, keel thickness $h = 0.4$ m and basin width $w_b = 1.5$ m. In addition, the indentor displacement $y_I$ and indentor force $F_I$ records from four repeated experiments are shown in both figures.

on ice rubble that was stirred few minutes before the experiments. In these experiments, it could be expected that the effect of freeze bonds was small, thus they were used for comparison. In Azarnejad and Brown (2001), shear strength values $\tau \approx 30 \ldots 100$ Pa were achieved with the indentor velocities used here. These values are on the same range with the values achieved here (30…150 Pa).

To derive $\tau$ in the Mohr–Coulomb model (see Eq. (1)), the failure process of the rubble has to fit the assumptions of the model. With ice rubble, it is assumed that the failure occurs on distinct shear planes which reach through the rubble thickness. This type of failure is called Mohr–Coulomb type (Azarnejad and Brown, 2000) and has been observed in laboratory scale ice rubble punch through experiments with low $v_I$. Clearly, the Mohr–Coulomb type of failure did not occur in the experiments here.

Anyhow, in laboratory punch through experiments with ice, the failure mode has been found to change with increasing $v_I$ (Azarnejad and Brown, 2001). As $v_I$ was increased, the Mohr–Coulomb type failure did not occur (Azarnejad and Brown, 2000, 2001; Brown and Lemee, 2002; Lemee and Brown, 2002). Instead, with high $v_I$ so called progressive failure occurs (Azarnejad and Brown, 2000). In progressive failure a volume of rubble with the shape of a wedge moves down with the indentor (Azarnejad and Brown, 2000). The change in the failure pattern has been reported occurring with indentor velocities 25…50 mm/s depending on the rubble type (Azarnejad and Brown, 2000; Brown and Lemee, 2002; Lemee and Brown, 2002). It should be noticed, that the progressive failure occurred with high $v_I$ even in rubble with freeze bonds.

The deformation pattern of the rubble described in Section 3.3.1 showed similar features with progressive failure with all $v_I$. In the experiments here, indentor load records did not show peak force corresponding to a breakage of a cohesive network. The similarity in the failure process suggests that the ice rubble in a punch through experiment with high $v_I$ might start to behave similarly to a rubble with no cohesion.

In the case of rubble with freeze bonds, the deformation of the rubble described in Section 3.3.1 would be expected to somewhat change. In this case, the rubble movement on top of the indentor (see (3b) in Fig. 19) would diminish due to the cohesion of the rubble.

### 4.2. Full scale vs. laboratory

In full scale experiments on ice, the effects due to experimental set up observed here do not occur. This is due to the typical preparation of a full scale test described in e.g. Heinonen (2004). As the illustration of a full scale experiment in Fig. 21 shows, a cut through the frozen layer of ice on top of the rubble has to be made to perform the punch through experiment on the rubble under the frozen layer. This procedure leads to a plug of ice moving down with the indentor during the experiment as illustrated in Fig. 21 b. The plug makes the effective indentor platen thickness to be related to the thickness of refrozen layer. In full scale, the maximum load $F_I^m$ is generally achieved with indentor displacements $y_I^m$, which are a fraction of the thickness of the plug.

Further in full scale, the displacement at submergence of the indentor platen is depended on the free board thickness shown in Fig. 21 a. If the free board thickness is larger than $y_I^m$, the effects related to indentor submergence reported here do not affect the value of the maximum load $F_I^m$. The value of $F_I^m$ in full scale is reached with relatively small $y_I^m$ and is believed to be dominated by the strength of the cohesive skeleton formed by freeze bond network between the blocks within the keel (see e.g. Heinonen, 2004).

For example, in full scale punch through experiments by Heinonen (2004), the plug of refrozen ice had thickness of 0.8 … 1.6 m, whereas the maximum force was achieved with less than 0.04 m of penetration. In those experiments, the free board was generally larger than

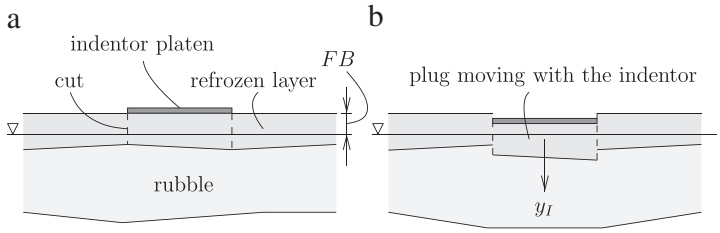


**Fig. 21.** Full scale punch through experiment before experiment (a) with a cut sawn through the refrozen layer of ice under the indentor for conducting the experiment on rubble mass. As shown in (b), during the experiment the plug of ice moves down with the indentor platen moving downwards into direction $y_I$. In (a), free board (*FB*) is shown.

$y_l^m$ (the only exception was one experiment, in which they report that no free board existed). Hence, $F_l^m$ was generally achieved before indentor submergence, and consequently, $F_l^m$ does not include effects due to the indentor submergence.

The experimental set up in laboratory experiments could be changed to better represent the set up in full scale. A simple enhancement would be to use thicker indentor platen to avoid the submergence of its total volume. It should be noted that the thickness of the indentor platen is likely related to both, the value of maximum load and the behavior of the rubble after the maximum load.

## 5. Conclusions

Laboratory scale punch through experiments on floating rubble consisting of plastic blocks were conducted. The motivation of using plastic blocks was to simplify the interpretation of results. In addition to the punch through experiments, a series of experiments with no rubble in the basin were performed. These experiments were conducted to estimate the hydrodynamical force $F_H$ induced by the experimental set up.

The effect of indentor velocity $v_I$ and the experimental set up on measured indentor force $F_I$ records were studied. Further, the derivation of material response and rubble shear strength (see Eq. (2)) from measured load histories were investigated. The main findings presented in the paper are:

- Maximum indentor load $F_l^m$ was always measured after the indentor had moved under the initial water level and was related to the hydrodynamic load acting on the indentor.
- With low indentor velocity $v_I$, the peak force in indentor force records was explained by hydrodynamic force $F_H$ measured from the open water experiments. Close to maximum indentor force $F_l^m$ in punch through experiments, the similarity of $F_I$ records was clear when compared to open water experiments.
- With high $v_I$, $F_I$ records also showed behavior related to $F_H$ close to $F_l^m$. However, fast decrease in $F_I$ after $F_l^m$ in punch through experiments continued even after the peak due to $F_H$. With increasing indentor displacement the rate of decrease changed. This behavior together with the observations on the rubble deformation (see Fig. 19 and Section 3.3.1) suggest that the $F_I$ records could be affected by the experimental set up.
- Due to effect of experimental set up, in fast experiments the rubble shear strength $\tau$ could become incorrectly estimated by Eq. (2).

The results thus suggest that the loading rate dependency observed in earlier laboratory punch through experiments with ice rubble could have been at least partly induced by the experimental set up instead of the rubble. In full scale, the experimental set up is very different from that in laboratory experiments. This could partly explain the differences in results of full scale and laboratory punch through experiments.

## Acknowledgments

The financial support from the Ministry of Education of Finland through the National Graduate School in Engineering Mechanics and from the Graduate Program of Aalto University, School of Engineering, is gratefully acknowledged. Authors would also like to thank Aalto University student Juhani Pennanen for his help in conducting the experiments.

## References

Azarnejad, A., Brown, T., 2000. Experimental investigation of ice rubble behaviour and strength in punch tests. Tech. Rep. 5–109, PERD/CHC.
Azarnejad, A., Brown, T., 2001. Small-scale plane strain punch tests. Journal of Cold Regions Engineering 15 (3), 135–153 September.
Azarnejad, A., Frederking, R., Brown, T., 1999. Ice rubble strength from small scale punch through tests. Proceedings of OMAE99, 19th International Conference On Offshore Mechanics and Artcic Engineering, pp. 1–9.
Brown, T., Lemee, E., 2002. Final report on experimental determination of ice rubble behaviour and strength. Tech. Rep. Report 5–115, PERD/CHC. February.
Bruneau, S., Crocker, G., McKenna, R., Croasdale, K., Metge, M., Ritch, R., Weaver, J., 1998. Development of techniques for measuring in situ ice rubble shear strength. Ice in Surface Waters, Proc. of the 14th International Symposium on Ice: IAHR, Vol. 2, pp. 1001–1007. Potsdam, New York, USA.
Croasdale, K.R., Bruneau, S., Christian, D., Crocker, G., English, J., Metge, M., Ritch, R., 2001. In-situ measurements of the strength of first-year ice ridge keels. Proceedings of the 16th International Conference on Port and Ocean Engineering under Arctic Conditions: POAC'01, Vol. 3, pp. 1445–1454. Ottawa, Ontario, Canada.
Ettema, R., Schaefer, J.A., 1986. Experiments on freeze-bonding between ice blocks in floating ice rubble. Journal of Glaciology 32 (112), 397–403.
Ettema, R., Urroz, G.E., 1989. On internal friction and cohesion in unconsolidated ice rubble. Cold Regions Science and Technology 16 (3), 237–247.
Faltinsen, O.M., 1990. Sea loads on ships and offshore structures. Cambridge Ocean Technology Series. Cambridge University Press.
Heinonen, J., 2004. Constitutive modeling of ice rubble in first-year ridge keel. Doctoral Thesis, TKK, VTT Publications 536. Espoo, Finland, 2004, 142 p, ISSN 1235–0621.
Heinonen, J., Määttänen, M., 2000. Ridge loading experiments, field experiments in winter 2000. LOLEIF Progress Report No. 10. TKK, 40 pp.
Heinonen, J., Määttänen, M., 2001a. Full-scale testing of ridge keel mechanical properties in loleif project. Proceedings of the 16th International Conference on Port and Ocean Engineering under Arctic Conditions: POAC'01, Vol. 3, pp. 1435–1444. August 12–17, Ottawa, Ontario, Canada.
Heinonen, J., Määttänen, M., 2001b. Ridge keel mechanical properties — testing. Field Experiments in Winter 2001. ReportSTRICE, TKK, 39 pp.
Jensen, A., Løset, S., Høyland, K.V., Liferov, P., Heinonen, J., Evers, K.-U., Määttänen, M., 2001. Physical modelling of first-year ice ridges — part II: mechanical properties. Proceedings of the 16th International Conference on Port and Ocean Engineering under Arctic Conditions: POAC'01, Vol. 3, pp. 1493–1502. Ottawa, Ontario, Canada.
Kuroiwa, D., 1961. A study of ice sintering. Tellus 13 (2), 252–259.
Lemee, E., Brown, T., 2002. Small-scale plane strain punch tests. Ice in the Environment: Proceedings of the 16th IAHR International Symposium on Ice.
Leppäranta, M., Hakala, R., 1992. The structure and strength of first-year ice ridges in the baltic sea. Cold Regions Science and Technology 20 (3), 295–311.
Liferov, P., 2005. Ice rubble behaviour and strength: part II. modelling. Cold Regions Science and Technology 41 (2), 153–163.
Liferov, P., Bonnemaire, B., 2005. Ice rubble behaviour and strength: part I. review of testing and interpretation of results. Cold Regions Science and Technology 41, 135–151.
Liferov, P., Jensen, A., Høyland, K., 2002. On analysis of punch tests on ice rubble. Proceedings of the 16th International Symposium on Ice, Vol. 2, pp. 101–110. Dunedin, New Zealand.
Liferov, P., Jensen, A., Høyland, K., 2003. 3D finite element analysis of laboratory punch tests on ice rubble. Proceedings of the 17th International Conference on Port and Ocean Engineering under Arctic Conditions: POAC'03, Vol. 2, pp. 611–621. Trondheim, Norway.
MATLAB, 2009. Version 7.9.0 (R2009b). The MathWorks Inc., Natick, Massachusetts.
Polojärvi, A., Tuhkuri, J., 2009. 3D discrete numerical modelling of ridge keel punch through tests. Cold Regions Science and Technology 56 (1), 18–29.
Tuhkuri, J., Polojärvi, A., 2005. Effect of particle shape in 2D ridge keel deformation simulations. Proceedings of the 18th International Conference on Port and Ocean Engineering under Arctic Conditions: POAC'05, Vol. 2, pp. 939–948. Potsdam, New York, USA.